




Enhancing the physical, optical and shielding properties for ternary $\text{Sb}_2\text{O}_3\text{--B}_2\text{O}_3\text{--K}_2\text{O}$ glasses

M. M. Soraya^{1,2,*} , Fatma. B. M. Ahmed^{1,2}, and M. M. Mahasen^{1,2}

¹Physics Department, Faculty of Science, Aswan University, Aswan, Egypt

²Academy of Scientific Research and Technology (ASRT), Cairo, Egypt

Received: 10 June 2022

Accepted: 18 August 2022

Published online:

15 September 2022

© The Author(s) 2022

ABSTRACT

Ternary $\text{Sb}_2\text{O}_3\text{--B}_2\text{O}_3\text{--K}_2\text{O}$ glass system, with general composition of $x \text{ Sb}_2\text{O}_3\text{--}(70\text{--}x) \text{ B}_2\text{O}_3\text{--}30 \text{ K}_2\text{O}$ (where $x = 0, 10, 20, 30, 40, 50$) were prepared using melt-quenching technique. Structures of these glasses were investigated using XRD analysis and FT-IR spectroscopy. The optical properties were investigated using the UV-Vis NIR JASCO (Model V-670) Double Beam Spectrophotometer. Different physical parameters, such as density (ρ), molar volume (V_M), oxygen molar volume (V_O) and oxygen packing density values (OPD) have been estimated. Also, the Gamma radiation shielding ability have been characterized for the investigated glasses using Phy-X/PSD software in the photon energy range (0.015–15 MeV). XRD analysis confirm the amorphous nature of the prepared glasses. The optical energy gap of SBK glasses is decreasing from 4 to 2.63 eV with increasing Sb_2O_3 content while refractive index is increasing from 2.17 to 2.5 because of increasing the non-bridging oxygens (NBOs) in the glass matrix. The molar refractivity (R_m), molar polarizability (α_m) and the third-order non-linear optical susceptibility values χ^3 have been calculated, their values are found to increase with increasing Sb_2O_3 content. Glass density and molar volume values for the SBK glasses increase with increasing Sb_2O_3 content. Increasing the Sb_2O_3 concentration enhance the radiation shielding features of the prepared glasses against gamma rays and neutrons. Hence, the mass attenuation coefficient (MAC) increases from 8.6 to 35.4 cm^2/gm while the half value layer (HVL) decreases from 0.036 to 0.0046 cm at 0.015 MeV as the Sb_2O_3 concentration increases from 0 to 50 mol%. The fast neutron cross section of the six investigated SBK glasses are (0.087, 0.092, 0.095, 0.091, 0.094 and 0.092 cm^{-1}), respectively.

Address correspondence to E-mail: somahmoud_81@yahoo.com

1 Introduction

Conventional glass formers such as phosphorus, silicon, boron, or germanium oxides is required and important in determining common oxide glass properties [1]. Heavy metal oxide glasses containing antimony, telluride, bismuth, tungsten, or lead have gained great interest and have preferred over the conventional glass because of their different advantages. They have high refractive index, low phonon energy, high thermal expansion and extended optical transmission spectrum [2–6]. Their attractive properties make them suitable candidate in many applications as optical amplifiers and non-linear optics components [2–6].

Antimony oxide-based glasses are considered one member of heavy metal oxide glasses family that was predicted by Zachariassen and confirmed by many authors [7–10]. These glasses gained significant interest in various technological applications as, nonlinear optical devices such as power limiters and ultra-fast optical switches [11, 12]. Pure Sb_2O_3 glasses was found to be a weak glass former and chemically unstable [13]. So, to enhance the vitrification behavior and to provide stabilization to the Sb_2O_3 network, it was preferable to incorporate the Sb_2O_3 with other conventional glass formers such as, SiO_2 [14], B_2O_3 [15], P_2O_5 [16, 17]. Antimony borate glasses have gained considerable interest because they can be applicable in the field of optics and electronics as a result of the heavy cations polarizability and the stereochemically alien lone pair of electrons present in the case of Sb^{3+} [18].

An important benefit of heavy metal oxide glasses (HMO) is to be used as shielding material against gamma-ray, x-ray and neutrons because of the high atomic number and density of heavy metals [19–24]. It was found that Sb_2O_3 improve the radiation attenuation properties of tellurite glasses containing V_2O_5 and Nb_2O_5 (TSVN) [19]. A.S. Abouhaswa et al. prove that Bi_2O_3 - B_2O_3 - Sb_2O_3 - Li_2O glasses (BSLB-glasses) have a higher photon protection capacity than ordinary (OC) and barite (BC) concretes [20]. Also it was found that MoO_3 improve the produced glass network compactness of alumino lead borate glasses and enhance the glass protection against neutrons [21]. G.A. Alharshan et al. studied the radiation-transmission and self-absorption factors of P_2O_5 - SrO - Sb_2O_3 glass system (PSS glass) [22], they found that some of PSS glasses are better than both

RS-253-G18 (standard commercial shield) and ordinary concrete in radiations shielding. K.C. Sekhar et al. investigated the effect of PbO on Bi_2O_3 - B_2O_3 - Fe_2O_3 glasses, they showed that their system is applicable for advanced optical and radiation shielding applications [23]. M. S. Al-Buriahi et al. studied the effect of heavy metal oxides (SrO , Al_2O_3 , CdO , ZnO , PbO and Bi_2O_3) on (TeO_2 - B_2O_3 - BaO - Er_2O_3) glasses, they found that these glasses are desirable shielding materials against gamma ray and neutrons [24].

In this work, ternary Sb_2O_3 - B_2O_3 - K_2O glass system was prepared and investigated. B_2O_3 was chosen as a good network former because it possesses high bond strength and low cation size. The addition of Alkali oxide (K_2O) modifies the glass network and transform tetrahedral (BO_4) units to trigonal (BO_3) units by the non-bridging oxygens formation [25]. Sb_2O_3 is added to standard glass formers to improve vitrification behavior, but it also raises phonon energy, which reduces infrared transmission [5, 6]. The current study's goal is to explore the Sb_2O_3 - B_2O_3 - K_2O glass. Since Sb has a larger atomic radius and density than B, this glass should have a higher refractive index, making it more appropriate for nonlinear optical applications. Additionally, Sb_2O_3 incorporation is anticipated to improve radiation shielding applications due to higher atomic weight and atomic number of Antimony compared to Boron. The glasses under investigation are with a general composition of (mol%) $x \text{Sb}_2\text{O}_3$ -(70-x) B_2O_3 -30 K_2O (where $x = 0, 10, 20, 30, 40, 50$). The Sb_2O_3 - B_2O_3 - K_2O glasses structure was investigated using XRD analysis and FT-IR spectroscopy. The optical properties were investigated using the UV-Vis-NIR JASCO (Model V-670) Double Beam spectrophotometer. The important parameters, such as density (ρ), molar volume (V_M), oxygen molar volume (V_O) and oxygen packing density values (OPD) have been estimated. Also, the Gamma radiation shielding ability have been characterized for the Sb_2O_3 - B_2O_3 - K_2O glasses using Phy-X/PSD software.

2 Experimental procedures

2.1 SBK glass preparation

The starting materials used in this work are B_2O_3 (99.9%), Sb_2O_3 (99.9%) and K_2O (99%), from Aldrich.

Ternary $\text{Sb}_2\text{O}_3\text{-B}_2\text{O}_3\text{-K}_2\text{O}$ glass system, with general composition of $x \text{ Sb}_2\text{O}_3\text{-(70-x) B}_2\text{O}_3\text{-30 K}_2\text{O}$ (where $x = 0, 10, 20, 30, 40, 50 \text{ mol\%}$) were prepared using melt-quenching technique. A mixture of the calculated composition batches was located in a ceramic crucible, and then heated in an electric furnace at $800 \text{ }^\circ\text{C}$ for 4 h, with continuous stirring to ensure melt homogeneity. The melt was then cast in air onto a brass mold, and the glass samples were annealed for 2 h at $200 \text{ }^\circ\text{C}$ to remove the mechanical stress that result from quenching. The obtained glass samples have been cut and polished into required shapes and sizes for different measurements. The label of the prepared glasses sample and their corresponding compositions are given in Table 1.

2.2 SBK glass characterizations

The XRD investigation was performed to emphasize the amorphous nature of the investigated glass samples. The XRD data for the powder glass samples was identified by X-ray diffractometer (D8 Discovery Bruker Company) at condition of 40 kV and 40AM (1600 W) at speed scan 0.01 P in the 2θ range from 10° to 80° , and with the aid of automated computer system. FT-IR spectroscopy analysis (type JASCO 430) was used to study the structure changes of investigated glass samples at room temperature and at spectral range $400\text{--}4000 \text{ cm}^{-1}$. The optical properties of the SBK glasses were investigated using the UV-Vis-NIR JASCO (Model V-670) Double Beam Spectrophotometer. A good polished SBK glass pellets of thickness 3 mm approximately was used. The spectra of the investigated glass were recorded at wavelength range $200\text{--}2500 \text{ nm}$. The Gamma radiation shielding

ability have been characterized for the $\text{Sb}_2\text{O}_3\text{-B}_2\text{O}_3\text{-K}_2\text{O}$ glasses using Phy-X/PSD software.

3 Results and discussions

3.1 SBK glasses formation domain and

In this work, ternary $\text{Sb}_2\text{O}_3\text{-B}_2\text{O}_3\text{-K}_2\text{O}$ glass system, with general composition of $x \text{ Sb}_2\text{O}_3\text{-(70-x) B}_2\text{O}_3\text{-30 K}_2\text{O}$ (where $x = 0, 10, 20, 30, 40, 50 \text{ mol\%}$) were prepared using melt-quenching technique. For visual inspection, as shown in Fig. 1 the SBK glasses look transparent for SBK1 and SBK2. The sample appearance changes with increasing the Sb_2O_3 content, the samples SBK3 and SBK4 show light yellow color. The samples with higher Sb_2O_3 contents, SBK5 and SBK6 are yellow colored. Figure 2 shows the glass forming domain for the ternary $\text{Sb}_2\text{O}_3\text{-B}_2\text{O}_3\text{-K}_2\text{O}$ system.

3.2 XRD structural studies for SBK glasses

The XRD analysis was performed for the SBK glass samples to examine the glass nature. The XRD data patterns for the SBK glass samples are shown in Fig. 3. For samples SBK1–SBK5, the absence for any sharp peaks and the presence of broad hump indicates the amorphous nature for these samples. The Sample SBK6 shows two sharp peaks at $2\theta = 14.74$ and 30.18 , which consistent with the diffraction planes (110), (022) of borate antimony oxide, respectively (COD 96–723-1902). The crystallization can be attributed to the large strengths difference between (F) B^{+3} ($F = 1.34$) and Sb^{+3} ($F = 0.73$) as the glass former content become closer (B_2O_3 and Sb_2O_3)

Table 1 Nominal composition and some optical properties of SBK glasses

$\chi^3(\text{esu})$	Molar polarizability $\alpha_m (\text{A}^3)$	Molar refractivity $R_m(\text{cm}^3 \text{ mol}^{-1})$	Optical energy gap (E_g) eV	Refractive index (n)	Compositions (mol %)			Sample label
					K_2O	B_2O_3	Sb_2O_3	
7.616E-13	7.535	18.989	4	2.17	30	70	0	SBK1
1.415E-12	8.012	20.191	3.52	2.27	30	60	10	SBK2
2.303E-12	8.532	21.501	3.21	2.343	30	50	20	SBK3
2.906E-12	9.627	24.259	3.08	2.376	30	40	30	SBK4
6.156E-12	10.164	25.613	2.73	2.474	30	30	40	SBK5
7.995E-12	11.123	28.03	2.63	2.505	30	20	50	SBK6

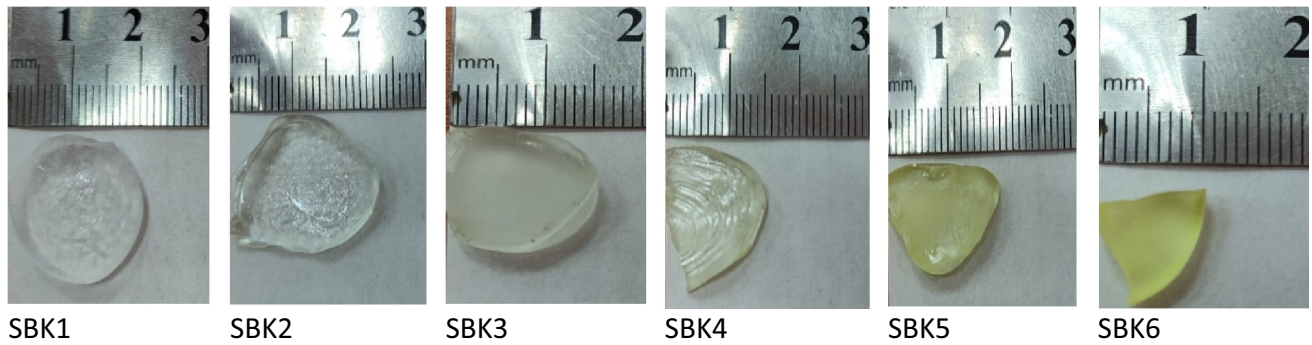


Fig. 1 Bulk SBK glass samples

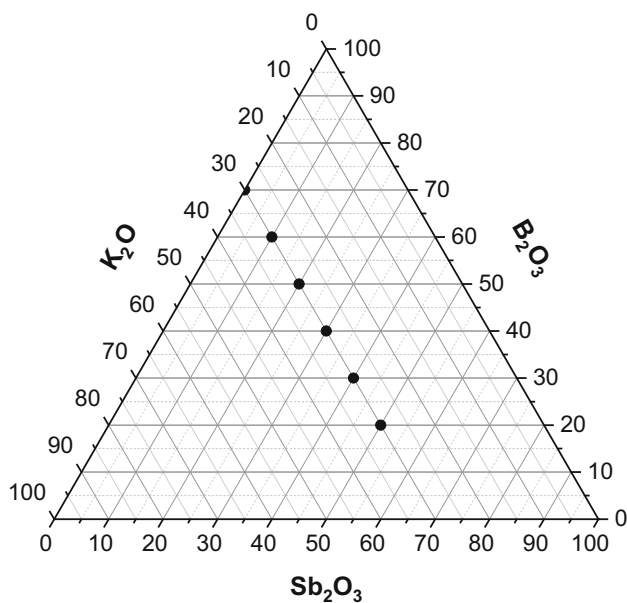


Fig. 2 Glass formation in the ternary $\text{Sb}_2\text{O}_3\text{-B}_2\text{O}_3\text{-K}_2\text{O}$ system (composition in mol%)

[13, 26–31]. The average crystallite size was evaluated from Debye–Scherrer’s equation as following [32]:

$$D = \frac{K\lambda}{\beta \cos \theta} \quad (1)$$

where D is the average crystalline size, θ is the diffraction angle, β is the peak width at half maximum height intensity, λ is the wavelength of the incident x-ray and K is the so-called Scherrer constant. K relies on the size distribution, shape, and indices of the diffraction line as well as the definition of β , whether it be FWHM or integral width [33]. K can have values anywhere from 0.62 and 2.08. In this paper, $K = 0.99$ was used. The average crystal size formed in SBK6 sample was found about 25 nm. Debye–Scherrer’s equation showed a good accuracy

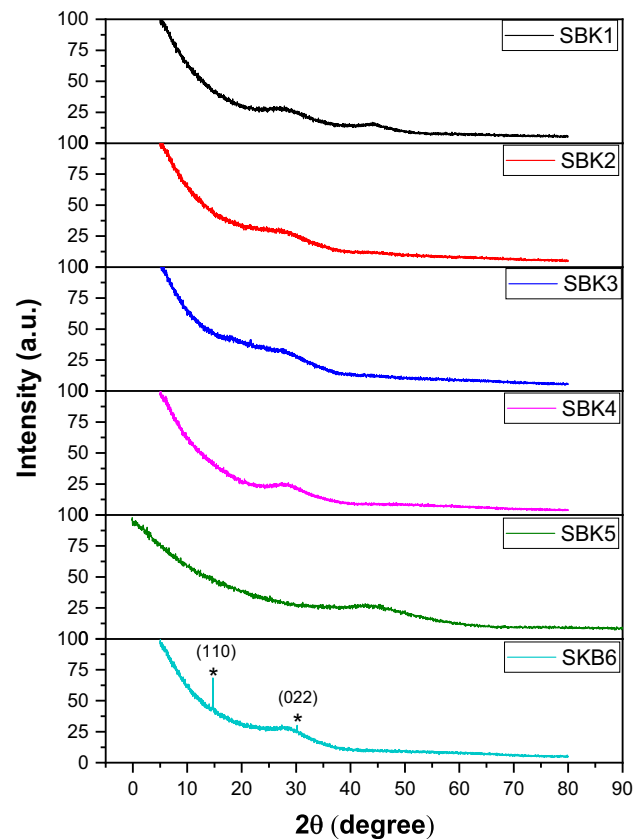


Fig. 3 X-ray diffractograms of **a** SBK1, **b** SBK2, **c** SBK3, **d** SBK4, **e** SBK5, **f** SBK6

in determination the crystallite size smaller than 100 nm as compared with other methods (Williamson–Hall method and the Rietveld refinement) [34], also in comparison with other techniques as transmission (TEM) and scanning electron microscopes (SEM) showed a good accuracy in estimating the small crystallite size less than 50–60 nm [34].

3.3 FT-IR analysis for SBK glasses

The structural properties of the SBK glasses were investigated by The Fourier transform IR (FT-IR) spectroscopy. The FT-IR spectra of SBK glasses in the spectral rang $400\text{--}4000\text{ cm}^{-1}$ is shown in Fig. 4. Figure 5 shows the FT-IR spectrum and the deconvolution of the FT-IR spectra of the SBK glasses. The deconvolution parameters and the band nature are presented in Table 2. The FT-IR spectra exhibited bands attributed to borate groups from ~ 1200 to $\sim 1500\text{ cm}^{-1}$ as a result of the asymmetric stretching vibration of the B–O–B bond of trigonal $[\text{BO}_3]$ units. Another band from $\sim 800\text{--}1200\text{ cm}^{-1}$ is resulting from the asymmetric stretching vibration of tetragonal $[\text{BO}_4]$ units. The band group $\sim 600\text{--}800\text{ cm}^{-1}$ is due to bending vibration of B–O–B linkages in the borate network [35, 36]. The band around $3000\text{--}3900\text{ cm}^{-1}$ is attributed to the hydroxyl groups, which indicates the presence of amount of water.

3.4 Optical properties of SBK glasses

The optical properties of the SBK glasses were investigated using the UV–Vis NIR JASCO (Model V-670) Double Beam spectrophotometer. The UV–vis absorbance spectra for the SBK glasses are shown in Fig. 6 (a). As shown in Fig. 1, the prepared SBK glass samples with low Sb_2O_3 content are transparent

(SBK1, SBK2 and SBK3) and they turn yellow for higher Sb_2O_3 content ones (SBK4, SBK5 and SBK6). As a result, it can be shown from Fig. 6 (a) that the absorbance increases with increasing the Sb_2O_3 for the SBK glasses. It can be noticed that the $\text{Sb}_2\text{O}_3\text{--B}_2\text{O}_3\text{--K}_2\text{O}$ glasses exhibit a good transparence for wavelengths longer than 400 nm . It also can be noticed that with increasing the Sb_2O_3 content, the UV absorption edge shifted into longer wavelengths (red shift).

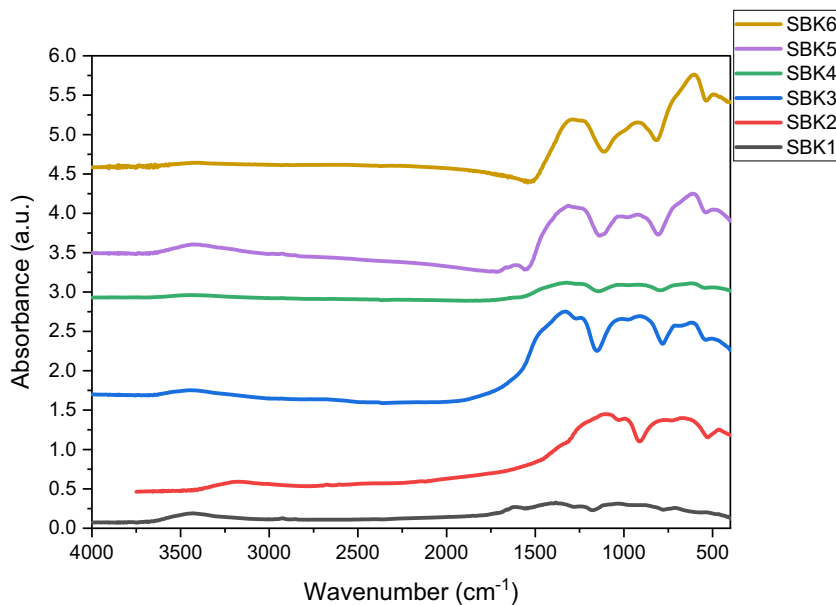
Generally, the UV region optical absorbance edge are used for understanding the optical transitions and the electronic band structure for materials. It is known that there are two types of optical transitions, direct and indirect transitions. The indirect optical energy gap (E_g) of the prepared SBK glass samples have been estimated using the optical absorption method. The absorption coefficient (α) of the glass samples can be calculated from the following relation [20]:

$$\alpha(\text{cm})^{-1} = 2.303(A/d) \quad (2)$$

Where A is the optical absorbance and d is the thickness of the SBK glass sample. The optical energy gap (E_g) of the SBK glasses was calculated using Tauc's relation as following [28–30]:

$$\alpha h\nu = B(h\nu - E_g)^2 \quad (3)$$

Fig. 4 FTIR spectra of SBK1–SBK6 samples



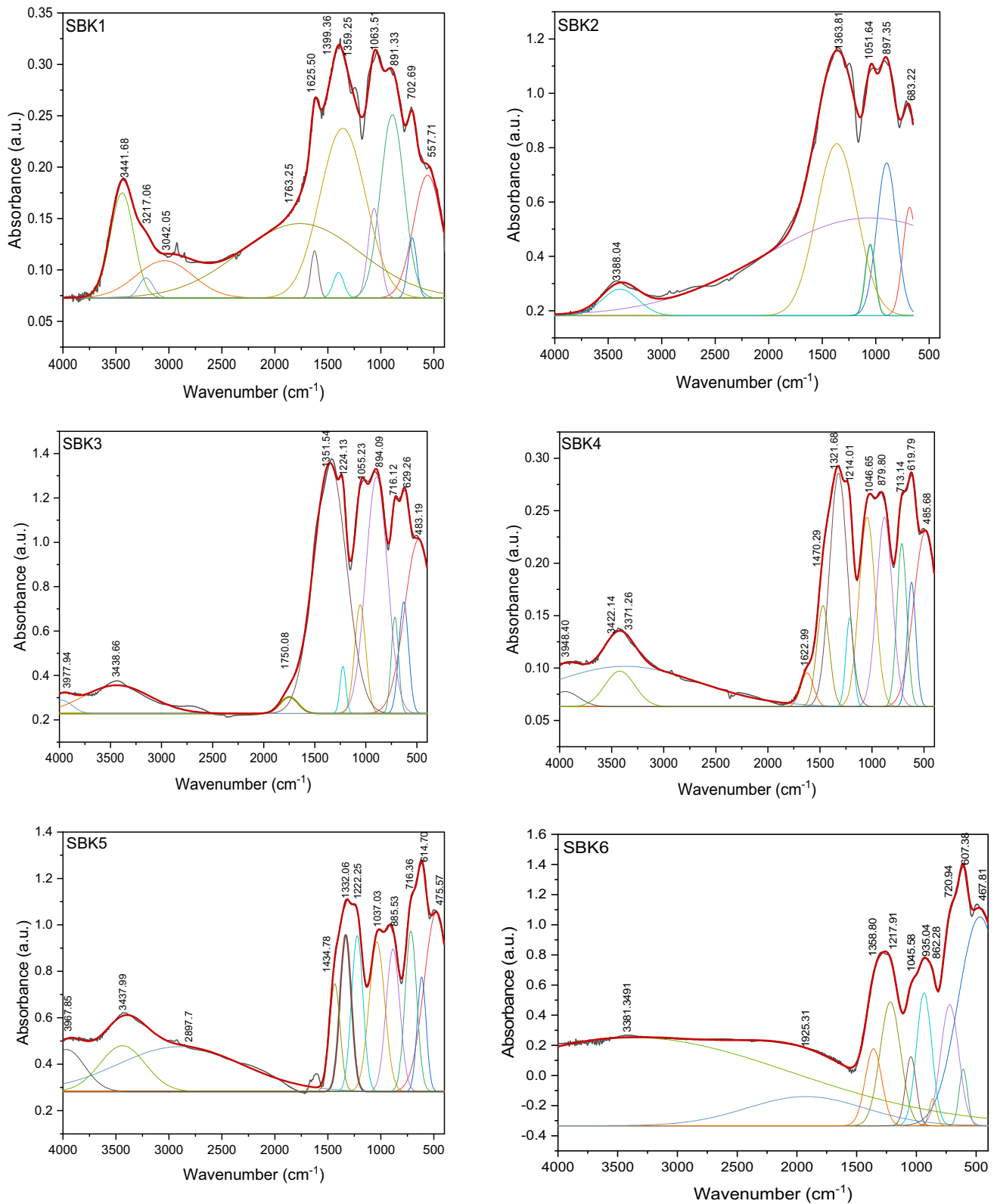


Fig. 5 Deconvolution of FTIR peaks for SBK glass samples (black line the raw data and the fitting viewed as a red line)

Table 2 FT-IRTS band position for SBK glasses with band assignment

Sample	Peak positions (cm ⁻¹)	Assignment
SBK1	557.71, 702.69, 891.33, 1063.51, 1359.25, 1399.36, 1625.50, 1763.25, 3042.05, 3217.06, 3441.68	
SBK2	683.22, 897.35, 1051.64, 1363.81	
SBK3	483.19, 629.26, 716.12, 894.09, 1055.23, 1224.13, 1351.54, 1750.08	
SBK4	485.68, 619.79, 713.14, 879.80, 1046.65, 1214.01, 1321.68, 1470.29, 1622.26	
SBK5	475.57, 614.70, 716.36, 885.53, 1037.03, 1222.25, 1332.06, 1434.78	
SBK6	467.81, 607.38, 720.94, 862.28, 1045.58, 1217.91, 1358.80	
	O–Sb–O bending modes, B–O–B vibration of B–O–B of tetragonal [BO ₄] units	
	asymmetric stretching of the B–O–B bond of trigonal [BO ₃] units	
	Hydrogen bonded OH (H–O–H)	
	Free hydroxyl group(O–H)	

where B is a constant, ν is the light frequency, h is the Planck's constant, E_g is the optical band gap.

The optical band gap energy (E_g) for the SBK glasses was estimated by extrapolating the linear part of the spectrum of $h \nu$ versus $(\alpha h \nu)^{1/2}$ as shown in Fig. 6b. Figure 7 shows the variation of the indirect optical energy gap (E_g) of the SBK glasses with the Sb_2O_3 content. It can be shown that the optical energy gap of SBK glasses is decreasing from 4 to 2.63 eV with increasing Sb_2O_3 content as shown in Table 1. This can be attributed to the increase in the non-bridging oxygens (NBOs) in the glass matrix with more Sb_2O_3 content [31].

The refractive index (n) is a very important parameters that affected the electromagnetic wave propagation of the material. The refractive index for the SBK glasses was estimated and related to the indirect optical energy gap (E_g) from the following equation [35].

$$\frac{(n^2 - 1)}{(n^2 + 2)} = 1 - \sqrt{\frac{E_g}{20}} \tag{4}$$

The variation of the refractive index values with the Sb_2O_3 content for the SBK glasses is presented in Fig. 8. As given in Table 1, (n) values vary from 2.17 for sample SBK1 and with increasing Sb_2O_3 content increase to 2.505 for SBK6. A higher value of refractive index value is obtained when the amount of nonbridging oxygen (which introduced by increasing the Sb_2O_3 content in our glass) is higher than the bridging oxygen in the glass samples [36]. This can attribute to those of the non-bridging oxygens (NBOs) which have large electronic hyperpolarizability character in comparison with the bridging oxygens.

The molar refractivity (R_m) and molar polarizability (α_m) have been calculated as following [37, 38]:

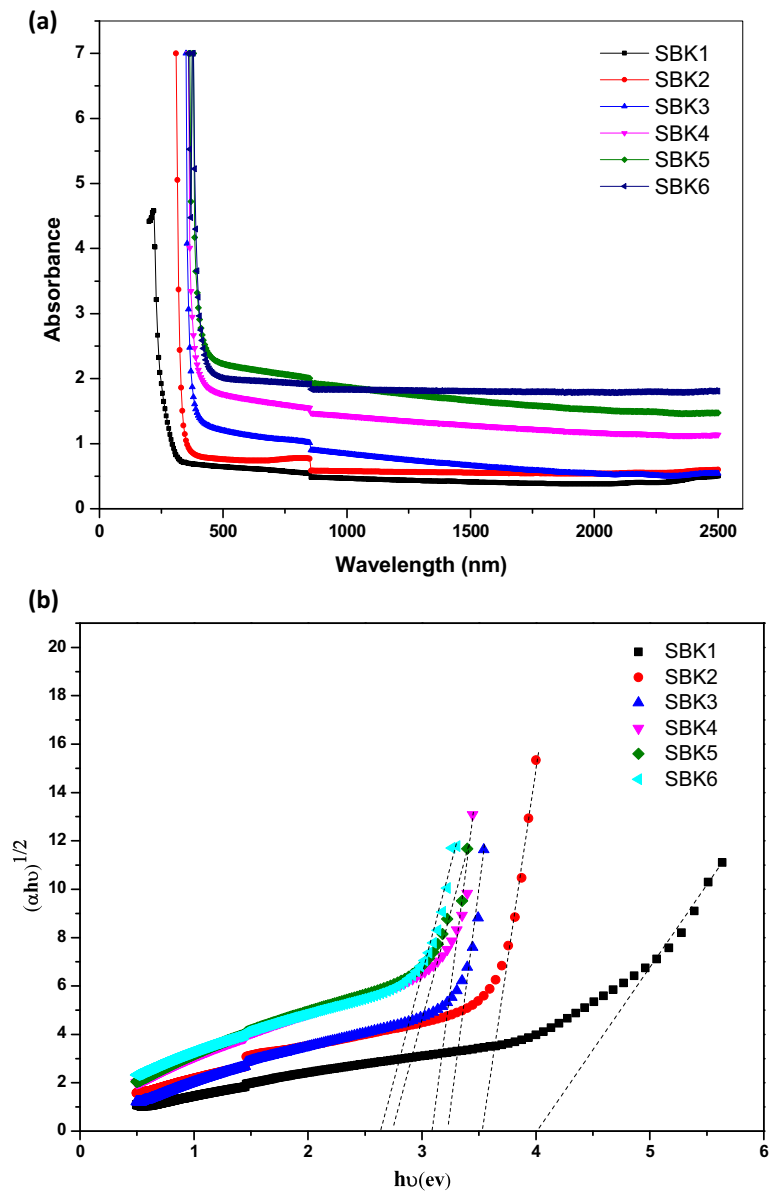
$$R_m = \left[\frac{n^2 - 1}{n^2 + 2} \right] V_m \tag{5}$$

$$\alpha_m = R_m / 2.52 \tag{6}$$

As shown in Table 1 for SBK glasses, the values of molar refractivity (R_m) and molar polarizability (α_m) are found to increase with increasing Sb_2O_3 content.

And, the optical energy gap values have been used to calculate the third-order nonlinear susceptibility χ^3 (in e.s.u units) as follows [39]:

Fig. 6 a Optical absorption spectra of SBK glass samples, **b** Tauc plots of SBK glass samples



$$\chi^3 = \frac{(1.4 \times 10^{-11})}{((E_g - 1.96))(E_g - 1.31)(E_g - 0.65)} \quad (7)$$

The values χ^3 for SBK glasses are listed in Table 1. It can be shown that the third-order nonlinear optical susceptibility values increase with increasing Sb_2O_3 content. This may be attributed to the decrease in the values of optical energy gap for the SBK glass samples. The samples SBK4, SBK5 and SBK6 show higher χ^3 values than that of pure silica glass (2.8×10^{-12} e.s.u), which means that the SBK samples with higher Sb_2O_3 content are promising for nonlinear optical devices.

3.5 Density, molar volume, oxygen molar volume and oxygen packing density.

The change in glass structure can be also investigated through estimation some of important parameters, such as density (ρ), molar volume (V_M), oxygen molar volume (V_O) and oxygen packing density values (OPD). These parameters consider a measure for any structure change as they are affected badly by structure softness, compactness, cross-linking, etc. For all the SBK glasses, the density was experimentally estimated and calculated through the Archimedes method. The measurements were performed at room temperature with the aid of a digital balance

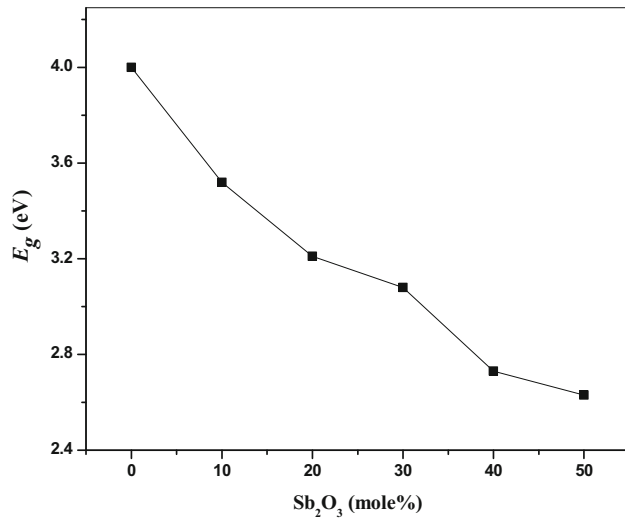


Fig. 7 Variation of optical energy gap (E_g) of SBK glasses with Sb_2O_3 percentage

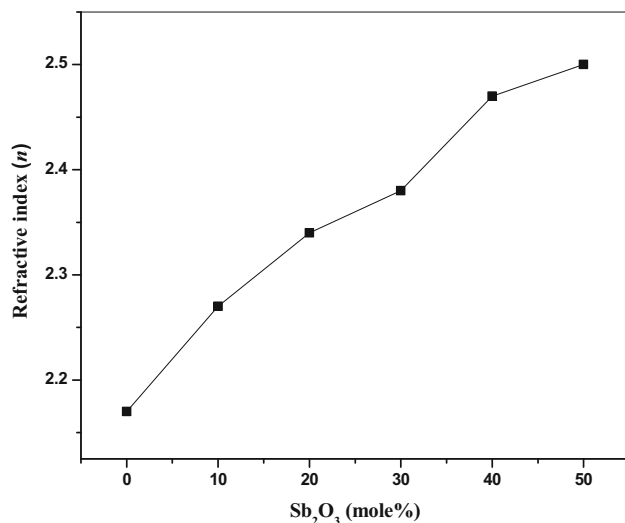


Fig. 8 Variation of refractive index (n) of SBK glasses with Sb_2O_3 percentage

of high sensitivity and using toluene with density 0.861 g/cm^3 as an immersion liquid. For each SBK glass sample, the average value of four separate measurements was taken to minimize the random error. The glass sample was weighted in air (W_{air}) and in toluene ($W_{toluene}$). The density (ρ_{exp}) was estimated using the following equation,

$$\rho_{exp} = \frac{W_{air}}{W_{air} - W_{toluene}} \quad (8)$$

Molar volume (V_M), Oxygen molar volume (V_O) and Oxygen packing density (OPD) of the SBK glasses were calculated as following:

$$V_M = \frac{M_{glass}}{\rho_{exp}} = \frac{\sum X_i M_i}{\rho_{exp}} \quad (9)$$

$$V_O = \frac{\sum X_i M_i}{\rho_{exp}} \frac{1}{\sum X_i n_i} \quad (10)$$

$$OPD = 1000C/V_M \quad (11)$$

M_i and X_i is the molecular weight and molar fraction of each component i respectively, n_i is the oxygen atoms number in each constituent oxide and C is the number of oxygen atoms at each glass composition [40, 41].

As shown in Fig. 9 the measured (ρ_{exp}) of the SBK glasses are found to increase with increasing the Sb_2O_3 concentration. The measured densities value varies from 2.241 gm/cm^3 for SBK1 sample to 4.273 gm/cm^3 for SBK6 sample as shown in Table 3. This increase in density value with increasing the Sb_2O_3 concentration can be a result of the replacement of Sb_2O_3 with high molecular mass (291.52 gm/mol) with B_2O_3 that has low molecular mass (69.62 gm/mol) [18]. As shown in Fig. 1 the glass color turns yellow with higher Sb_2O_3 , which also indicated the glass density change.

Figure 9 also depicted the molar volume values for the SBK glasses that were estimated according to the Eq. (9) using the measured densities. It's obvious that the molar volume (V_M) also increases with increasing

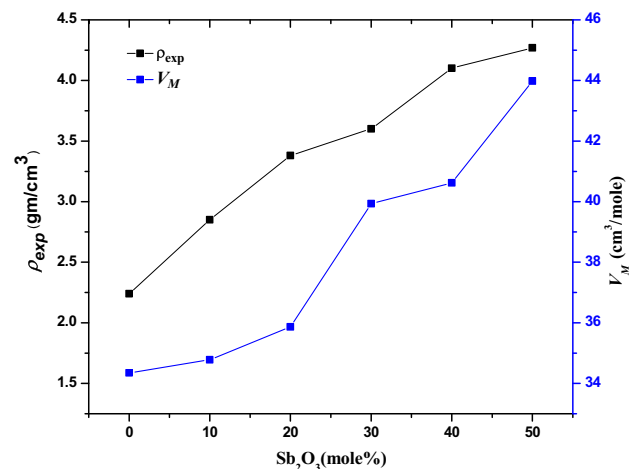
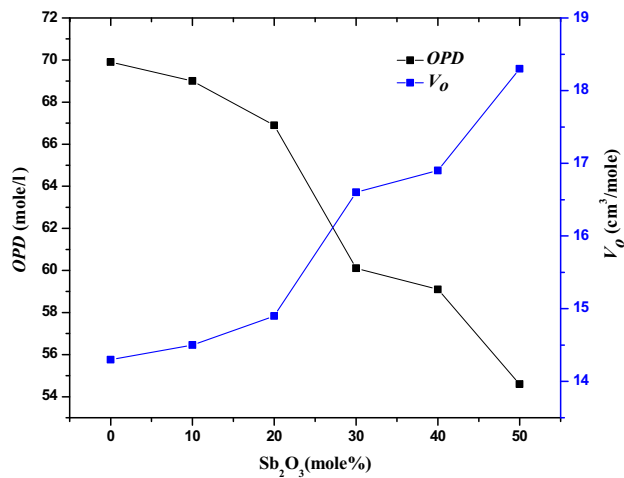


Fig. 9 Variation of the measured density (ρ_{exp}) and molar volume (V_M) values of SBK glasses with Sb_2O_3 content

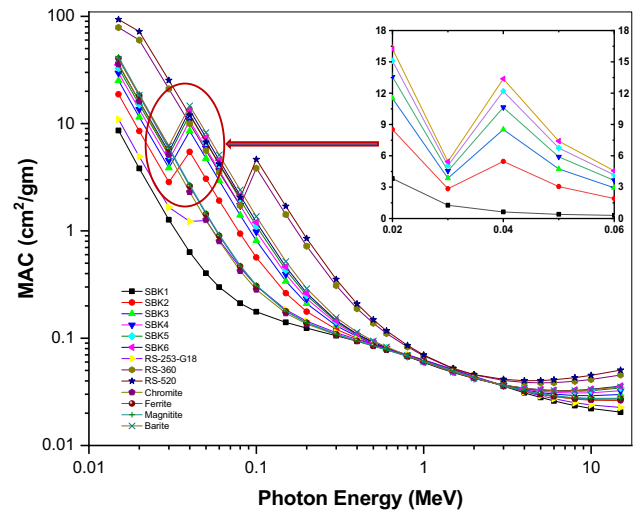
Table 3 Some physical properties of SBK glasses

Sample label	ρ_{exp} (g/cm ³)	ρ_{theor} (g/cm ³)	V_M (cm ³ /mol)	V_O (cm ³ /mol)	OPD (mol/l)
SBK1	2.241±0.001	2.48	34.35	14.3	69.9
SBK2	2.851±0.001	2.79	34.78	14.5	69
SBK3	3.383±0.002	3.11	35.87	14.9	66.9
SBK4	3.595±0.003	3.42	39.93	16.6	60.1
SBK5	4.08±0.003	3.73	40.62	16.9	59.1
SBK6	4.273±0.002	4.04	43.98	18.3	54.6

**Fig. 10** Variation of oxygen molar volume (V_O) and oxygen packing density (OPD) of SBK glasses with Sb_2O_3 content

Sb_2O_3 concentration, and they were varied from 34.35 for SBK1 to 43.98 (cm³/mol) for SBK6 (represented in Table 3). This increase in molar volume values for the SBK glasses can attributed to larger ionic size of Sb^{3+} (76 pm) ions compared to that of B^{3+} (23 pm) [18] and to the larger bond length of Sb-O (1.932 Å) compared to the bond length of B-O (1.372 Å) [42].

The variation of both oxygen molar volume (V_O) and oxygen packing density (OPD) values with Sb_2O_3 concentration is depicted in Fig. 10. The oxygen molar volume value shows increase with increasing the Sb_2O_3 concentration, their values vary from 14.3 cm³/mol for SBK1 to 18.3 cm³/mol for SBK6 (showed in Table 3). While the oxygen packing density (OPD) decrease with increasing the Sb_2O_3 concentration, their values vary from 69.9 mol/l for SBK1 to 54.60 mol/l for SBK6 as shown in Table 3. The (OPD) decrease because of increasing the molar volume (V_M), hence the Oxygens number remain the same by substituting B_2O_3 with Sb_2O_3 .

**Fig. 11** (MAC) parameter values for SBK glasses in comparison with MAC of other traditional and commercial glasses as a function of photon energy

The theoretically predicted densities (ρ_{theor}) were calculated using the densities of the glass sample constituent oxides according to their appropriate concentrations as follows:

$$\rho_{theor} = \sum X_i \rho_i \quad (12)$$

where i is the index of the oxide; X_i and ρ_i are the molar fraction and density of the i th oxide, respectively. As shown in Table 3, the theoretically predicted density is also increase with increasing the Sb_2O_3 concentration as we mentioned above because of the higher atomic mass of Sb_2O_3 compared to that of B_2O_3 . The theoretically predicted density value varies from 2.48 gm/cm³ for SBK1 sample to 4.04 gm/cm³ for SBK6 sample. The experimental density shows higher value than the theoretical one, except in SBK1 (the behavior is reversed). To clarify this manner, we should look to the molar volume of

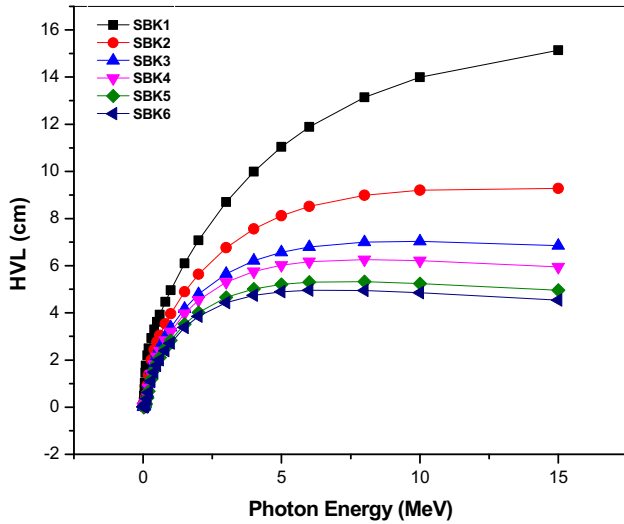


Fig. 12 (HVL) parameter values for SBK glasses versus photon energy

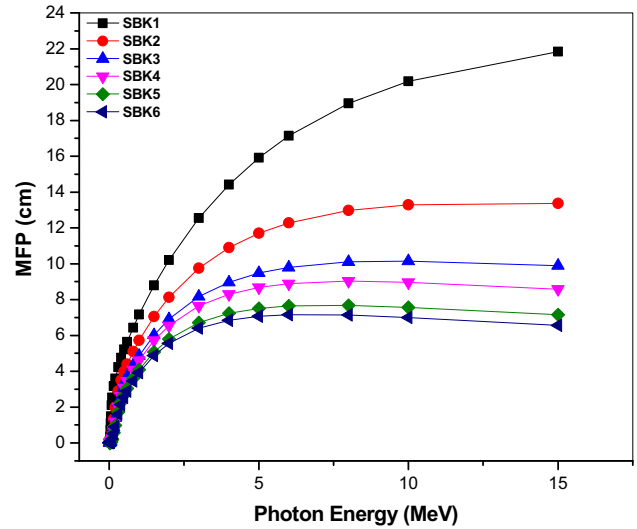


Fig. 14 (MFP) parameter values for SBK glasses versus photon energy

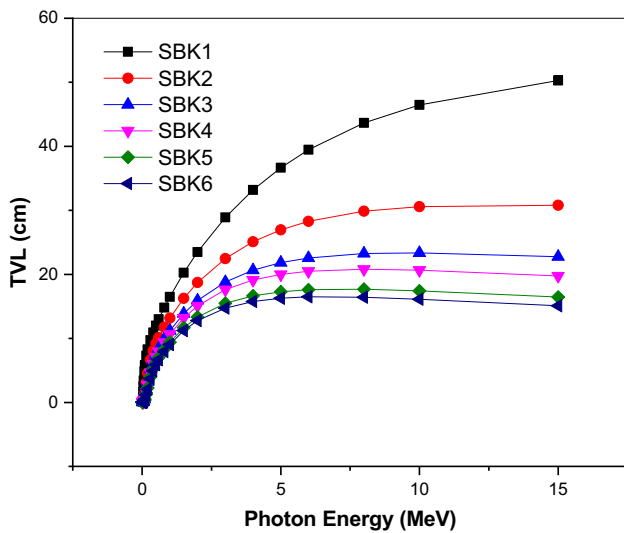


Fig. 13 (TVL) parameter values for SBK glasses as a function of photon energy

each constituting oxide separately, in the present investigation the B_2O_3 (molar volume = $27.3 \text{ cm}^3/\text{mol}$) is replaced with the Sb_2O_3 (molar volume = $51.4 \text{ cm}^3/\text{mol}$). From the measured molar volume of the SBK glasses V_m , we found that V_m increases slowly with increasing Sb_2O_3 content in the glass since it varies between 34.35 and $43.98 \text{ cm}^3/\text{mol}$. This means that Sb_2O_3 is more coordinated in the glass structure, which resulted in increasing the measured density in comparing with the theoretically predicted one.

3.6 Radiation shielding properties of SBK glasses

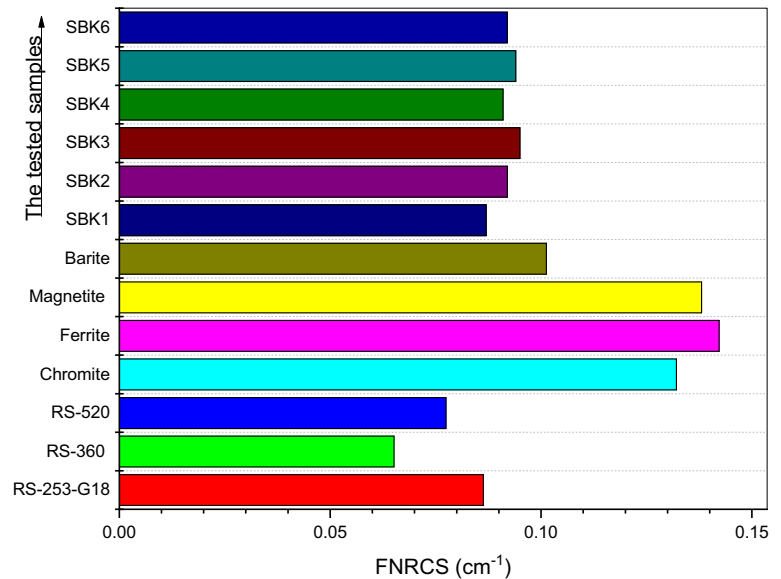
Some shielding parameters have been evaluated using Phy-X/PSD online software [43] to characterize the Gamma radiation shielding ability for SBK glasses. The mass attenuation coefficient, MAC , is very important parameter that characterize the probability of photons to interact the glasses and it is the basic tool to estimate the different shielding parameters and can be calculated with the known of glass density (ρ) as following [43, 44]:

$$\mu_m = \left(\frac{\mu}{\rho}\right) = \sum_j w_j \left(\frac{\mu}{\rho}\right)_j \tag{13}$$

Figure 11 shows the MAC of the SBK glasses in the photon energy ranged from 0.015 to 15 MeV . As shown in Fig. 11, MAC values of some traditional and commercial glasses are also included for comparison. For all the SBK glasses show an exponentially decrease in MAC value, with a sharp decrease indicating in the 0.015 – 0.1 MeV range. Sample SBK1 exhibits the lowest MAC value, and with increasing the Sb_2O_3 concentration for (SBK2-SBK6) glasses the MAC value increases. Hence, MAC increases from 8.6 to $35.4 \text{ cm}^2/\text{gm}$ at 0.015 MeV as the Sb_2O_3 concentration increases from 0 to $50 \text{ mol}\%$. The great influence of Sb_2O_3 content and the highest recorded MAC values at low energies (0.015 – 0.1 MeV), were due to the photon interaction processes. The K-absorption

Table 4 Photon energies (in MeV) of absorption edges and atomic number Z of the constituent elements under investigations [45]

Element	Z	$M1$	$L3$	$L2$	$L1$	K
K	19	—	—	—	—	3.60740E-03
Sb	51	—	4.13220E-03	4.38040E-03	4.69830E-03	3.04912E-02
B	5	—	—	—	—	—

Fig. 15 The fast neutron removal cross section, $FNRCS$ of the studied glasses (SBK1-SBK6) in comparison with $FNRCS$ of other traditional and commercial glasses

edge effect which arise from photoelectric effects can be seen at 0.04 MeV of photon energy which is nearly close to the K-absorption edge of Sb (as shown in Table 4, which represents the absorption edges and atomic numbers of the constituent elements of the investigated glasses [45]), which resulted the discontinuity in the attenuation curve for (SBK2-SBK6) glasses. SBK6 sample has MAC values close to that of the Barite and higher MAC values than that of some commercial (RS-253-G18) and ordinary glasses (Ferrite, Chromite and magnetite), which means that SBK6 sample is the best for shielding applications among the investigated SBK glasses.

The tenth (TVL) and half-value layer (HVL) also are two important parameters, to determine the glass thickness required to can attenuate the radiation intensity to about 10% and 50% of its initial intensity, respectively [43]. They can be calculated as following:

$$HVL = \frac{\ln(2)}{\mu}, TVL = \frac{\ln(10)}{\mu} \quad (14)$$

The mean free path (MFP) is a significant parameter to characterize the glass radiation shielding feature, lower MFP value is the best for radiation shielding and it can be evaluated as following [43]:

$$MFP = \frac{1}{\mu} \quad (15)$$

Figures 12, 13 and 14 show the values of (HVL), (TVL) and (MFP) of the SBK glasses, respectively. For all the SBK glasses both the (HVL), (TVL) and (MFP) values increase with increasing photon energy and decrease with increasing the Sb_2O_3 concentration. Hence, HVL decreases from 0.036 to 0.0046 cm at 0.015 MeV as the Sb_2O_3 concentration increases in SBK1 to SBK6 glasses; which indicate that increasing the Sb_2O_3 concentration enhance the radiation shielding feature of the prepared glasses. It has been concluded that the SBK6 glass sample is the best between SBK investigated glasses for radiation shielding because it has the smallest HVL , TVL and MFP value, since it possesses the highest density.

Furthermore, the fast neutron removal cross section ($FNRCS$) (ΣR) is a factor used to characterize

how far the material is capable to attenuate neutrons. Nuclear fission, neutron capture, nuclear spallation processes, and elastic and inelastic scattering are some of the ways that neutrons and matter may interact. The following equation may be used to calculate the *FNRCs* (*R*) parameter, which is used to gauge a material's neutron attenuation capacity [43, 44]:

$$\sum R = \sum_i \rho_i \left(\sum R/\rho \right)_i$$

Here, $(\Sigma R/\rho)_i$ and ρ_i are the mass removal cross section (*MRCs*) and partial density of the *i*th constituent element, respectively. The *MRCs* values were according to the literatures [46, 47]. The estimated values of *FNRCs* are illustrated in Fig. 15, the *FNRCs* values of SBK1, SBK2, SBK3, SBK4, SBK5 and SBK6 glasses are 0.087, 0.092, 0.095, 0.091, 0.094 and 0.092 cm⁻¹, respectively. It is shown by the graph that *FNRCs* of the investigated glasses are higher and, therefore, better for neutrons protection than some commercial glasses (RS-253-G18, RS-520 and RS-360).

4 Conclusions

The influence of Sb₂O₃ on the optical, physical, and structural properties was investigated for the ternary Query Sb₂O₃–B₂O₃–K₂O glass system. The SBK glass sample with low Sb₂O₃ content is transparent and it turn yellow for higher Sb₂O₃ content. The optical energy gap of SBK glasses is decreasing from 4 to 2.63 eV with increasing Sb₂O₃ content due to the increase in the non-bridging oxygens (NBOs) in the glass matrix with more Sb₂O₃ content. The refractive index values vary from 2.17 for sample SBK1 and with increasing Sb₂O₃ content increase to 2.505 for SBK6.

The molar refractivity (*R_m*), molar polarizability (*α_m*) and the third-order nonlinear optical susceptibility values χ^3 have been calculated. Their values are found to increase with increasing Sb₂O₃ content. Densities, molar volume, oxygen molar volume of the SBK glasses are found to increase with increasing the Sb₂O₃ concentration, while oxygen packing density decreases. Glass sample with higher Sb₂O₃ concentration is the best between the studied SBK glasses for radiation shielding. Hence, SBK6 sample has higher *MAC* values than that of some commercial (RS-253-

G18) and ordinary glasses (Ferrite, Chromite and magnetite).

Acknowledgements

This work was produced with the financial support of the Academy of Scientific Research and Technology of Egypt; ScienceUP/GradeUp initiative: Grant Agreement No (6451). Its contents are the sole responsibility of the authors and do not necessarily reflect the views of the Academy of Scientific Research and Technology.

Authors contributions

M. M. Soraya: Conceptualization, Methodology, Investigation, Data Curation, Data analysis, Writing-Review. Fatma. B. M. Ahmed: Writing—Original Draft, Writing – Review. M. M. Mahasen: Conceptualization, Methodology, Investigation, Data Curation, Data analysis, Writing-Review.

Funding

This work was funded by the Academy of Scientific Research and Technology of Egypt; ScienceUP/GradeUp initiative: Grant Agreement No (6451). Open access funding provided by The Science, Technology & Innovation Funding Authority (STDF) in cooperation with The Egyptian Knowledge Bank (EKB).

Data availability

Data are available under author request.

Declarations

Conflict of interest The authors declare there is no conflicts of interest.

Open Access This article is licensed under a Creative Commons Attribution 4.0 International License, which permits use, sharing, adaptation, distribution and reproduction in any medium or format, as long as you give appropriate credit to the original author(s) and the source, provide a link to the Creative Commons licence, and indicate if changes were made. The images or other third party material in this

article are included in the article's Creative Commons licence, unless indicated otherwise in a credit line to the material. If material is not included in the article's Creative Commons licence and your intended use is not permitted by statutory regulation or exceeds the permitted use, you will need to obtain permission directly from the copyright holder. To view a copy of this licence, visit <http://creativecommons.org/licenses/by/4.0/>.

References

1. W.H. Zachariasen, *J. Am. Chem. Soc.* **54**, 3841–3851 (1932)
2. W.H. Dumbaugh, J.C. Lapp, *J. Am. Ceram. Soc.* **75**(9), 2315–2326 (1992)
3. D. Lezal, J. Pedlikova, P. Kostka, J. Bludaska, M. Poulain, J. Zavadil, *J. Non Cryst. Solids*. **284**(1–3), 288–295 (2001)
4. J.A. Ruller, J.E. Shelby, *Phys. Chem. Glas.* **33**(5), 177–183 (1992)
5. T. Som, B. Karmakar, *J. Non Cryst. Solids*. **356**(20–22), 987–999 (2010)
6. K. Terashima, T. Hashimoto, T. Uchino, S.H. Kim, T. Yoko, *J. Ceram. Soc. JAPAN* **104**(11), 1008–1014 (1996)
7. A.E. Ersundu, M.C. Ersundu, N. Gedikoglu, *J. Non Cryst. Solids* **541**, 10093 (2020)
8. S.Y. Marzouk, F.H. Elbatal, *J. Mol. Struct.* **1063**, 328–335 (2014)
9. A.E. Ersundu, M. Celikbilek, M. Baazouzi, M.T. Soltani, J. Troles, S. Aydin, *J. Alloys. Compd.* **615**, 712–718 (2014)
10. J.S. Roy, Y. Messaddeq, S.J.L. Ribeiro, *J. Mater. Sci.: Mater. Electron.* **30**(18), 16798–16805 (2019)
11. M. Hamzaoui, M.T. Soltani, M. Baazouzi, B. Tioua, Z.G. Ivanova, R. Lebullenger, M. Poulain, J. Zavadil, *Phys. Status Solidi B*. **249**(11), 2213–2221 (2012)
12. K. Ouannes, K. Lebbou, B.M. Walsh, M. Poulain, G. Alombert-Goget, Y. Guyot, *Opt. Mater.* **65**, 8–14 (2017)
13. T. Som, B. Karmakar, *J. Am. Ceram. Soc.* **92**(10), 2230–2236 (2009)
14. S. Gandi, S.S.S. Panda, S.R. Parne, M. Lakavat, N.R. Lakkimsetty, S.S. Gandi, *J. Mater. Sci.: Mater. Electron.* **32**(22), 26709–26715 (2021)
15. H. Doweidar, K. El-Egili, R. Ramadan, M. Al-Zaibani, *J. Non-Cryst. Solids*. **497**, 93–101 (2018)
16. M. Nalin, Y. Messaddeq, S.J.L. Ribeiro, M. Poulain, V. Briois, G. Brunklaus, C. Rosenhalm, B.D. Mosel, H. Eckert, *J. Mater. Chem.* **14**(23), 3398–3405 (2004)
17. B. Zhang, Q. Chen, L. Song, H.P. Li, F.Z. Hou, J.C. Zhang, *J. Non-Cryst. Solids* **354**(18), 1948–1954 (2008)
18. G. Jagannath, B. Eraiah, A. Gaddam, H. Fernandes, D. Brazete, K. Jayanthi, K.N. Krishnakanth, S.V. Rao, J.M.F. Ferreira, K. Annapurna, A.R. Allu, *J. Phys. Chem. C* **123**(9), 5591–5602 (2019)
19. M.S. Al-Buriahi, H.H. Hegazy, F. Alresheedi, H.H. Somaily, C. Sriwunkum, I.O. Olarinoye, *Appl. Phys. A: Mater. Sci. Process.* **127**, 2 (2021)
20. A.S. Abouhaswa, I.O. Olarinoye, N.V. Kudrevatykh, E.M. Ahmed, Y.S. Rammah, *J. Mater. Sci.: Mater. Electron.* **32**(9), 12439–12452 (2021)
21. M.S. Al-Buriahi, Z.A. Alrowaili, I. Kebaili, A.M. Al-Baradi, E.A.A. Wahab, I.O. Olarinoye, C. Sriwunkum, K.S. Shaaban, *Phys. Scr* **96**, 12 (2021)
22. G.A. Alharshan, C. Eke, M.S. Al-Buriahi, *Radiat. Phys. Chem.* **193**, 109938 (2022)
23. K.C. Sekhar, A. Hameed, N. Narsimlu, J.S. Alzahrani, M.A. Alothman, I.O. Olarinoye, M.S. Al-Buriahi, M. Shareefuddin, *Opt. Mater.* **117**, 111173 (2021)
24. M.S. Al-Buriahi, J.S. Alzahrani, I.O. Olarinoye, H. Akyildirim, S. Alomairy, I. Kebaili, H.O. Tekin, C. Mutuwong, *Phys. Scr* **96**, 7 (2021)
25. M.K. Halimah, W.H. Chiew, H.A.A. Sidek, W.M. Daud, Z.A. Wahab, A.M. Khamirul, S.M. Iskandar, *Sains Malaysiana* **43**(6), 899–902 (2014)
26. K.J. Rao, *Structural chemistry of glasses*, Elsevier (2002)
27. R.B. Rao, N.O. Gopal, N. Veeraiah, *J. Alloys. Compd.* **368**(1–2), 25–37 (2004)
28. J. Tauc, A. Menth, *J. Non-Cryst Solids*. **8–10**, 569–585 (1972)
29. K. Pal, J.S. Roy, T.P. Majumder, S. Ghosh, S.K. Roy, R. Schirhagl, R. Dabrowski, *J. Lumin.* **136**, 278–284 (2013)
30. J.S. Roy, T.P. Majumder, C. Schick, *J. Mol. Struct.* **1088**, 95–100 (2015)
31. S. Rani, S. Sanghi, N. Ahlawat, A. Agarwal, *J. Alloys. Compd.* **597**, 110–118 (2014)
32. S. Paul, *Nachr. Ges. Wiss. Göttingen.* **26**, 98–100 (1918)
33. J.I. Langford, A. Wilson, *J. Appl. Crystallogr.* **11**(2), 102–113 (1978)
34. V. Uvarov, I. Popov, *Mater. Charact.* **85**, 111–123 (2013)
35. R. El-Mallawany, M.D. Abdalla, I.A. Ahmed, *Mater. Chem. Phys.* **109**(2–3), 291–296 (2008)
36. Y.B. Saddeek, K.A. Aly, A. Dahshan, I.M. El Kashef, *J. Alloys. Compd.* **494**(1–2), 210–213 (2010)
37. V. Dimitrov, S. Sakka, *J. Appl. Phys.* **79**(3), 1736–1740 (1996)
38. B. Eraiah, *Bull. Mater. Sci.* **33**(4), 391–394 (2010)
39. T. Tasheva, V. Dimitrov, *J. Chem. Technol. Metall.* **52**(2), 369–378 (2017)
40. M. Celikbilek, A.E. Ersundu, S. Aydin, *J. Non-Cryst Solids* **378**, 247–253 (2013)

41. A.E. Ersundu, M. Celikbilek, N. Solak, S. Aydin, J. Eur. Ceram. Soc. **31**(15), 2775–2781 (2011)
42. O.C. Gagne, F.C. Hawthorne, Acta. Crystallogr. B. Struct. Sci. Cryst. Eng. Mater. **74**, 63–78 (2018)
43. E. Şakar, Ö.F. Özpolat, B. Alim, M.I. Sayyed, M. Kurudirek, Radiat. Phys. Chem. **166**, 108496 (2020)
44. Z.M.H. El-Qahtani, E.R. Shaaban, M.M. Soraya, Chalcogenide Lett. **18**(6), 311–326 (2021)
45. J.H. Hubbell, S.M. Seltzer, No. PB-95-220539/XAB; NISTIR-5632 (1995)
46. A.B. Chilton, J.K. Shultis, R.E. Faw, Principles of radiation shielding, United States: N. p. (1984)
47. M.F. Kaplan, Concrete radiation shielding, United States: N. p. (1989)

Publisher's Note Springer Nature remains neutral with regard to jurisdictional claims in published maps and institutional affiliations.